A Compact Low-Loss Broadband Polarization Independent Silicon 50/50 Splitter

Devika Padmakumar Nair and Michaël Ménard, *Member, IEEE*

***Abstract*—We present a low-loss, compact, polarization insensitive 3-dB optical power-splitter for submicron silicon waveguides. The splitter is optimized over a broad wavelength span ranging from 1300 to 1700 nm through finite difference time domain simulations. The splitter junction footprint is only 1.8 × 1.3 μm, which is smaller than previously reported broadband multimode junction splitters. Furthermore, the demonstrated device overcomes the fabrication limitations of previous splitters while maintaining a compact size without any sharp angles. The device was fabricated using electron beam lithography. The experimental results show a small insertion loss of less than 0.3 dB for both the TE and TM polarizations.**

***Index Terms*—Silicon photonics, splitter, multimode interferometer.**

I. Introduction

SILICON photonics is a promising field because of the high-density of devices that can be built on a single chip [1]–[5]. Compact and low-loss splitters are critical in photonics circuits since they are frequently used in light distribution or as component to build devices such as optical switches [6], multiplexers [7], or modulators [8]. Recently, optical 3-dB power splitters with enhanced performance have been demonstrated using Y-junctions [9], [10], directional couplers (DC) [11]–[13], adiabatic couplers [14]–[18] and multimode interference (MMI) couplers [19]–[25]. Nevertheless, these approaches still face a number of limitations. Y-junctions are the most compact integrated power splitters and also have a polarization insensitive response. However, the sharp junctions and small feature size of Y-junction splitters are challenging to build due to the resolution limits of commercial fabrication processes, and small fabrication variations can give rise to significant scattering loss. Furthermore, DC-based splitters are highly sensitive to wavelength and coupling length variations. They can be improved with asymmetrical structures [26] but the overall size of DC-based splitters is typically very large. Most adiabatic couplers are long and not compatible with CMOS fabrication processes because of their minimum feature size [15], [16]. MMI-based splitters based on the self-imaging effect can achieve low losses and are tolerant to fabrication variations. Self-imaging is a feature of multimode waveguides where an input field profile is reproduced or replicated in single or multiple images at a fixed interval along the propagation direction [27]. However, typical MMI-based splitters are polarization dependent and devices relying on the excitation of a large number of high order modes suffer from compression of their bandwidth [25]. The large footprint of MMI-based splitters can also be an issue, particularly in compact integrated systems. Y. Zhang *et al.* demonstrated a low-loss and compact splitter in which they modified the junction shape [9]. The measured insertion loss of this Y-splitter is less than 0.3 dB but this design was optimized only for the TE polarization in the 1500 to 1580 nm wavelength range [9]. In 2013, Z. Xiao *et al*. demonstrated a low-loss, polarization insensitive MMI splitter with a junction footprint of 1.5 × 1.8 μm [25]. However, this device requires a silicon core with a thickness of 330 nm, which is larger than the standard thickness (220 nm) used in most commercial fabrication processes [25]. Thus, the power splitter designs reported so far in the literature are limited by at least one impediment, such as coupling losses created by mode mismatch at output arms of splitter, high sensitivity to wavelength and/or polarization, or a large footprint. Moreover, many compact designs are difficult to fabricate in commercial silicon photonic foundries because of their small features.

In this work, we report the design, fabrication and characterization of a splitter structure with a carefully designed small multimode region that controls the evolution of the optical field and the number of excited modes to minimize losses, maximize the operational wavelength range, and reduce sensitivity to polarization. This design is compact, and it overcomes the fabrication limitations of previously designed splitters. Moreover, it operates without exciting a large number of higher order modes in the multimode junction. Simulations are performed over a wide wavelength range of 1300 nm to 1700 nm for both polarizations. The device was successfully fabricated using electron beam lithography and tested using an automated test station.

II. Design and Optimization

We used both analytical expressions and numerical simulations to design of the power splitter. Fig. 1(c) shows the schematic of a typical MMI coupler, which was our starting point. The approximate length of the MMI, L_{MMI}, for a 1 × 2

Manuscript received May 30, 2021; accepted June 18, 2021. Date of publication June 22, 2021; date of current version July 8, 2021. This work was supported in part by the Fonds de Recherche du Québec - Nature et Technologies (FRQNT)2018-PR-208814, and in part by the Natural Sciences and Engineering Research Council of Canada under Grant 418352/2012, centre d'optique photonique et laser. *(Corresponding author: Devika Padmakumar Nair.)*

Devika Padmakumar Nair is with the Department of Electrical Engineering, École de Technologie Supérieure, Montréal, QC H3C 1K3, Canada (e-mail: devika.padmakumar-nair.1@etsmtl.net).

Michaël Ménard is with the Microtechnology and Microsystems Laboratory, Université du Québec à Montréal, Montréal, QC H3C 3P8, Canada (e-mail: menard.michael@uqam.ca).

Digital Object Identifier 10.1109/JPHOT.2021.3091539

This work is licensed under a Creative Commons Attribution 4.0 License. For more information, see https://creativecommons.org/licenses/by/4.0/

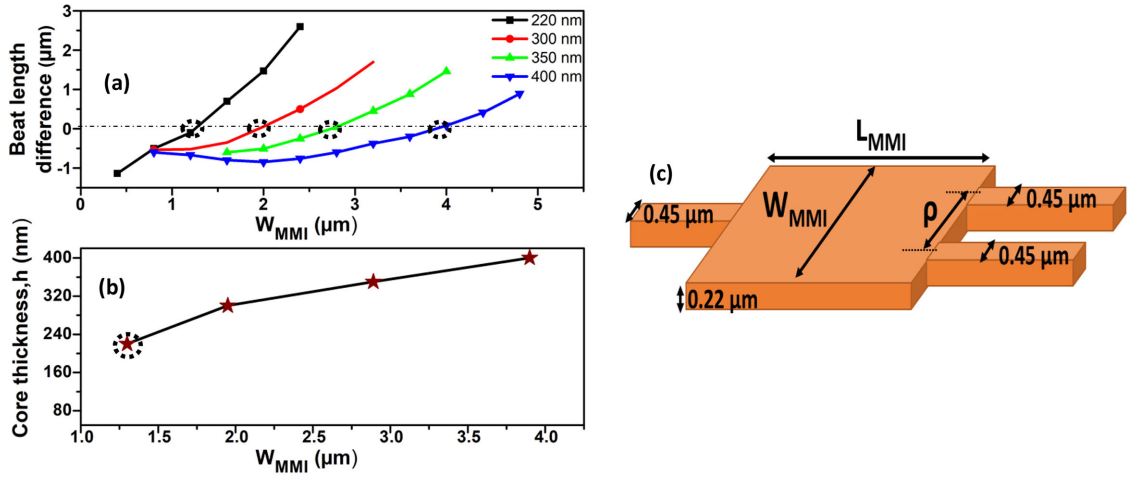

Fig. 1. (a) Change in the beat length difference between the TE and TM polarizations as a function of the width of the MMI for different core thicknesses, (b) optimal MMI width (at $\Delta\, \mathrm{L}\pi = 0$) as a function of the core thickness, (c) schematic of a typical 1×2 MMI structure.

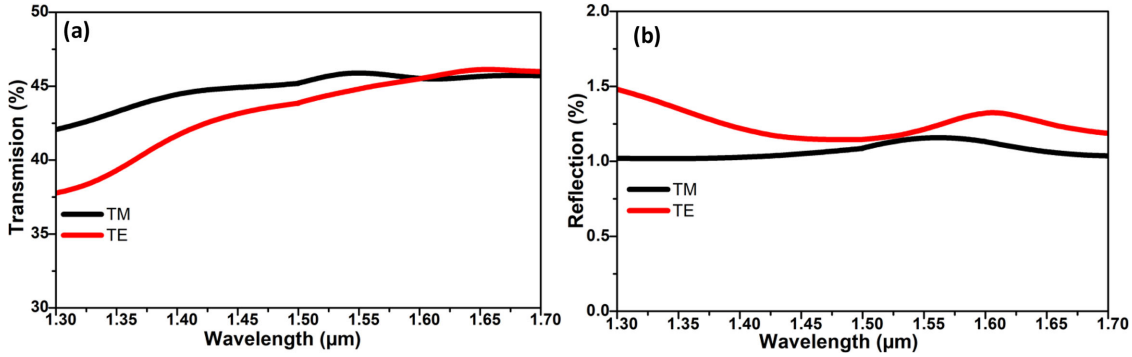

Fig. 2. (a) Simulated power transmission spectrum and (b) simulated reflection spectrum of the optimized MMI coupler for the TE and TM polarizations.

splitter is calculated with the following equation [26]:

$$\mathrm{L_{MMI}} = (3\mathrm{L}_\pi)/4\mathrm{N} \tag{1}$$

Where N is the number of images of the input (or number of outputs) at the end of the MMI, L_π is the beat length, which is obtained from $L_\pi = \pi/(\beta_0\text{-}\beta_1)$, and β_0 and β_1 are the lowest order modes propagation constants, which are calculated using a finite difference Eigenmode solver. To design a polarization insensitive MMI splitter, the beat length difference between the two polarizations ($\Delta\, L_\pi$) should be zero, i.e.:

$$\Delta \mathrm{L}_\pi = \Delta \mathrm{L}_{\pi(\mathrm{TE})} - \Lambda\, \mathrm{L}_{\pi(\mathrm{TM})} = 0 \tag{2}$$

Fig. 1(a) shows the change in beat length difference between the TE and TM polarizations (ΔL_π) as a function of the width of the MMI (W_{MMI}) for different core thicknesses (h). The MMI is polarization insensitive when its width fulfills the $\Delta L_\pi = 0$ condition for that particular core height. It is clear that as W_{MMI} becomes larger, the beat length difference between the two polarizations increases rapidly. Fig. 1(b) demonstrates that the width at which the MMI is polarization insensitive increases with the core height of the waveguide. The core height of single mode silicon waveguides is generally smaller than 500 nm. Here, we focus on the design of a 1×2 MMI coupler with a core height of 220 nm and thus the width at which the coupler is polarization insensitive is 1.3 μm, as shown in Fig. 1(b). The length of the MMI coupler for $N = 2$ (considering the first two lower order modes) is calculated with Eq. (1) to be 1.25 μm. This is only an approximation since the mode might not be strictly confined into the core of the multimode region [28]. In a MMI with N ports, N equally spaced images are formed at the output. The distance between the images is referred to as the pitch and is given by $\rho = \mathrm{W_{MMI}}$ /N. In this design, the calculated pitch is 0.65 μm, which will prevent crosstalk between the output waveguides. Hence, the separation between the inner edges of the output waveguides is 0.2 μm. The normalized transmitted and reflected power as a function of wavelength for the MMI splitters designed based on the analytical equations is plotted in Fig. 2(a) and (b). The device is simulated over a wide wavelength range from 1300 nm to 1700 nm.

The size and shape of the multimode waveguide section was modified further to minimize reflections and scattering losses created by sharp corners. The performance was improved by analyzing the field distribution inside the device using the finite difference time domain (FDTD) simulation software by Lumerical. The outcome is that the optimized MMI region is now shaped

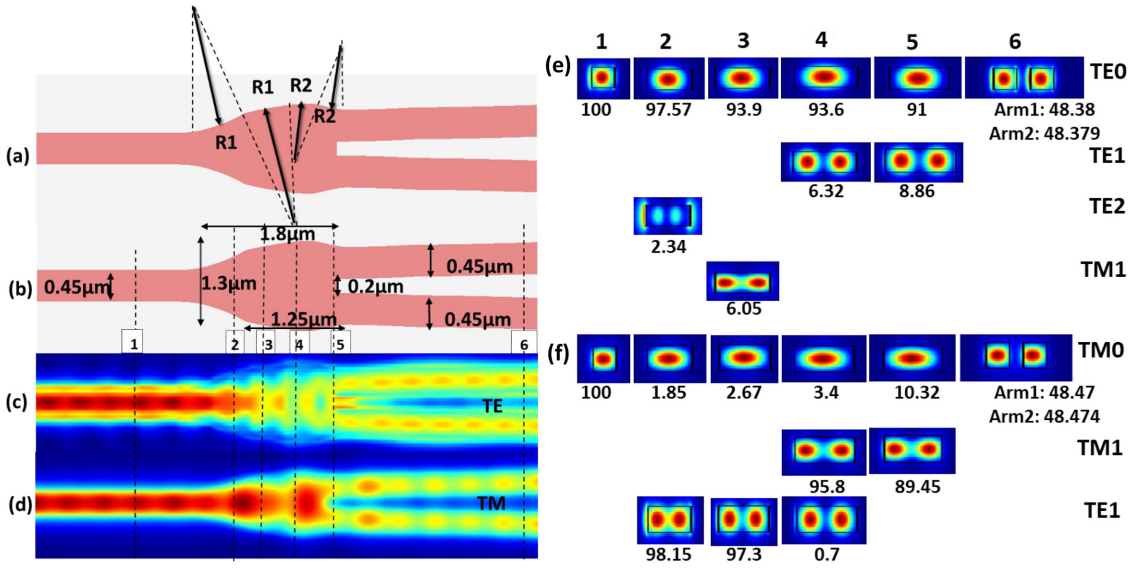

Fig. 3. (a), (b) Optimized splitter geometry. Intensity profile of the splitter for (c) TE polarization and (d) TM polarization. (e) and (f) illustrate the mode profile and mode percentage for the TE and TM polarizations at the cross sections identified as 1, 2, 3, 4, 5 and 6.

into two consecutive S-bends with radius R1 and R2 as illustrated in Fig. 3(a). The optimized design is obtained by gradually increasing R1 from 0.5 µm to 1.6 µm and R2 from 0.45 µm to 1 µm. The final radii of the S-bends for a symmetric splitter are R1 = 1.4 µm and R2 = 0.8 µm. This smoothen the sharp corners and maximizes the transmission at the output of the MMI for both polarizations. While smoothening the shape of the MMI, we also aimed to maximize the operational wavelength range of the splitter. The final MMI based splitter geometry is shown in Fig. 3(b). The total length and width of the reshaped multimode region is only 1.8 µm × 1.3 µm. The width of the MMI region gradually increases from 0.45 µm to 1.3 µm and then narrows down to 1.1 µm at the output. The gradual increase of the width at input end of the MMI region reduces reflection losses at the junction. This also improve the self-image quality and reduces propagation losses by limiting the number of higher order modes that are excited to those below the TE_2 and TM_2 modes. The field profile and cross-sectional mode profiles were calculated at a wavelength of 1550 nm to clearly understand how the splitter operates. Fig. 3(c) and 3(d) show the field intensity distribution of the TE and TM polarization along the device. There is no significant excitation of radiation modes in the device, as the TE and TM modes are well confined in the silicon waveguide. Cross sectional mode profiles of the TE and TM excited modes along the device, including the percentage of incident power coupled to each mode for different cross sections (1 to 6) are illustrated in Fig. 3(e) and (f). The fraction of power transmitted into each mode travelling in the cross section is calculated using the finite-difference eigenmode solving algorithm. Overlap integrals are performed between each mode and the simulated field in order to determine the fraction of power that is travelling in a specific mode [29]. Interestingly, not only are a few modes excited inside the junction but there is even some polarization conversion since the TE light couples briefly to the TM_1 mode and TM light does the same with the TE_1 mode. However, the power in both output waveguides as the same polarization state as the input signal. Moreover, the modulation of the intensity between sections 2 and 5 in Fig. 3(c) and (d) resulting from the interference between the modes excited in the multimode region demonstrates that the splitter is still operating based on the self-imaging principle after modifying the junction shape. For both polarizations, the power splits uniformly and couples efficiently to the two output waveguides (Fig. 3(e) and (f), section 6). The final splitter design, including the input waveguide, MMI region and the two bend waveguides at the output end of MMI, occupies a very small area of 18 µm × 4 µm, which is similar or significantly less than that of other state-of-the-art designs [9], [10], [25]. The minimum feature size is 200 nm, which is compatible with the design rules of commercial silicon photonic fabrication processes.

The simulated transmission and reflection spectra of the optimized splitter along with simulated results for a rectangular MMI splitter with similar dimensions are shown in Fig. 4. The optimized splitter achieves a very high transmission efficiency of 46.5 to 49% for each output port for both the TE and TM polarizations over the wavelength range 1300 nm–1700 nm (Fig. 4(a)). A very small back reflection of less than 0.70% for the TE polarization and 0.55% for the TM polarization was observed (Fig. 4(b)), which creates small ripples in the field intensity of the input waveguide (see Fig. 3(c, d) before section 2). If we compare the transmission results of the optimized splitter and standard MMI splitter, the optimized one shows on average an improvement in performance of 6-7% over the wavelength range from 1300 nm to 1700 nm. Furthermore, the response of the optimized splitter is almost wavelength insensitive over the range 1450 nm-1700 nm, with a variation below 0.5%. The simulated insertion loss at a wavelength of 1550 nm is approximately 0.11 dB for both the TE and TM polarizations. It is clearly noticeable that the losses for the TE polarization increases for the lower wavelength, whereas for the TM

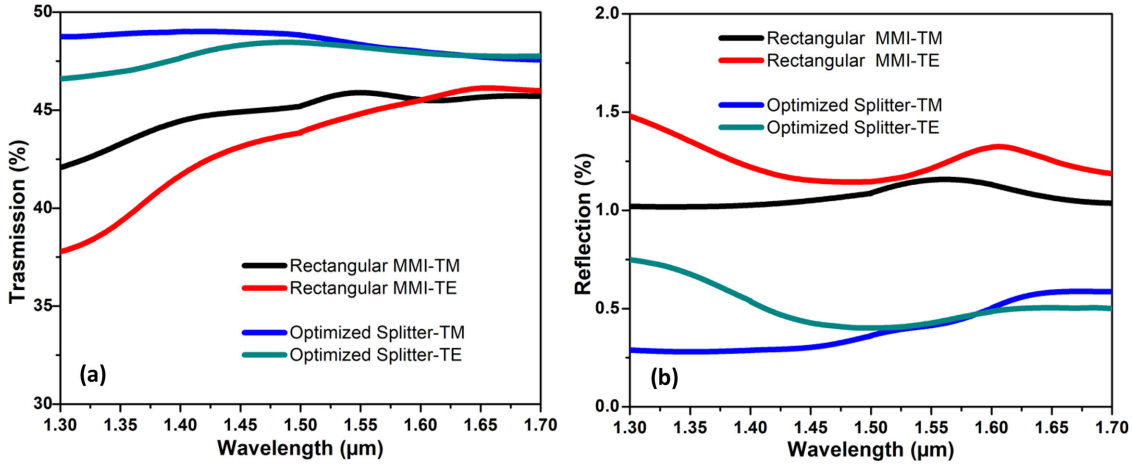

Fig. 4. (a) Simulated power transmission for a rectangular MMI and the optimized splitter for both polarizations. (b) Simulated back reflection in a rectangular MMI and the optimized splitter for both polarizations.

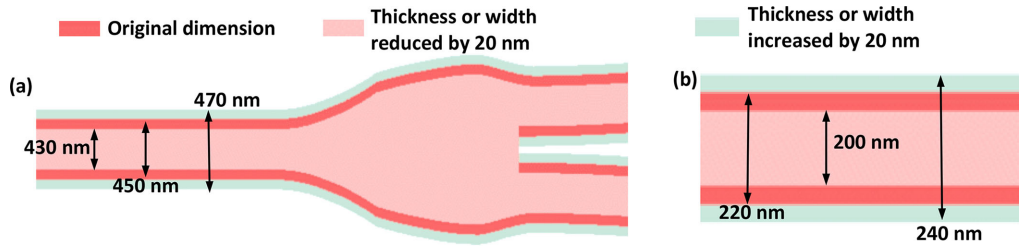

Fig. 5. (a) Optimized splitter geometry with ± 20 nm width variation. (b) Optimized splitter geometry with ± 20 nm thickness variation.

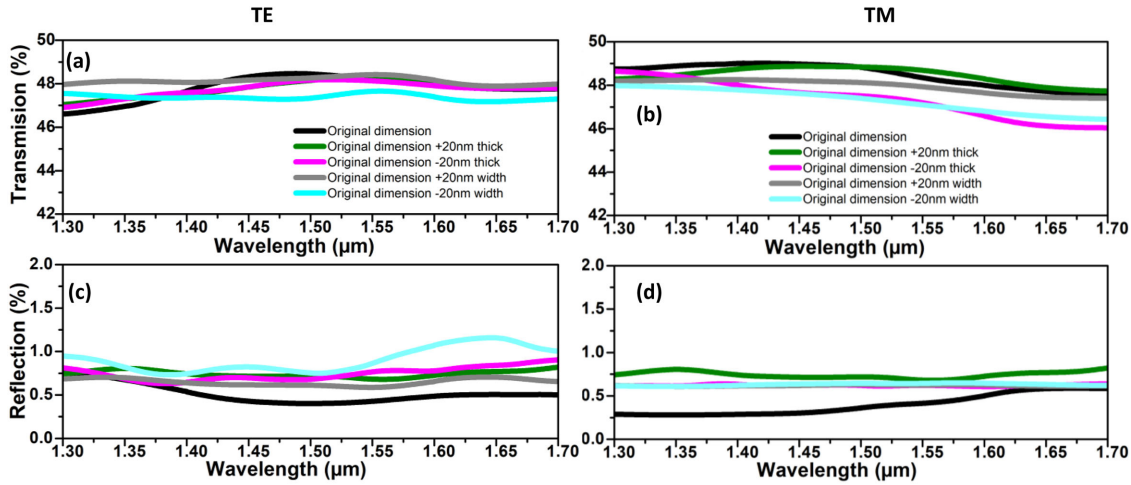

Fig. 6. (a,b) Simulations comparing of the power transmitted in each arm of the optimized splitter when fabricated with its original dimensions and when its width or thickness varies by ± 20 nm for (a) the TE and (b) TM polarization. (c, d) Simulated back reflections in the optimized splitter when fabricated with its original dimensions and when its width or thickness vary by ± 20 nm for (c) the TE and (d) TM polarization.

polarization the performance increases at lower wavelengths. Note that the impact of sidewall roughness is not considered in the simulations.

The performance of splitters can be sensitive to geometry variations, notably in the thickness of the silicon film and in the width of the device [9]. The fabrication tolerances of the device were evaluated by changing its thickness and width by ±20 nm and then simulating its performance. Fig. 5(a) illustrates the impacts of variations in width and Fig. 5(b) those of variations thickness. The transmission and reflection spectra of the original geometry and of those including the variations in dimensions are presented in Fig. 6. For the TE polarization the transmission fluctuates by about 1% around the value for the nominal design (see Fig. 6(a)) whereas for the TM polarization (see Fig. 6(b)) the

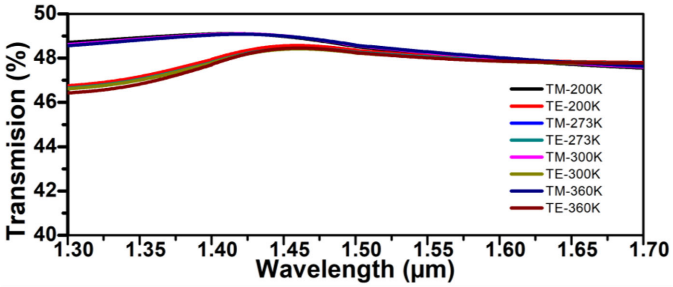

Fig. 7. Simulated power transmission at different temperature.

transmission varies by around 0.5% for increases in thickness or width. However, reduction in width or thickness induce losses of around 1.8%. Therefore, the performance of the device is resilient to variations in dimensions according to the simulation results.

The performance of the splitter is not expected to vary significantly with temperature. To characterize its temperature dependence, the splitter is simulated for temperatures ranging from 200K to 360K (see Fig. 7). The variation of transmission at output port is less than 0.2% for TM and less than 0.35% for TE polarization over the entire wavelength range, indicating that the device is almost temperature insensitive.

III. Fabrication and Characterization

The devices were fabricated using electron beam lithography at two facilities: the University of Washington and Applied Nanotools. The starting substrates were 25 mm squares diced from wafers with a 220 nm thick silicon device layer on a 3 μm thick buried silicon dioxide (SiO_2) layer. After spin coating hydrogen silsesquioxane resist and a hot plate bake, electron beam lithography was performed using an energy of 100 keV followed by resist development. The silicon was removed from the unexposed area using plasma etching. In the end, a cladding of 2 μm of SiO_2 was deposited with plasma enhanced chemical vapor deposition.

Different sets of structures were fabricated to experimentally characterize the splitter including cascades of Mach-Zehnder interferometers (MZI) (Number of splitters, Ns = 0, 56, 112) to determine the insertion loss (IL), a single splitter to determine splitting ratio and an independent MZI to measure its extinction ratio (ER). The case where Ns = 0 in Fig. 8(a) is only two grating couplers (GCs) connected by same number of bent waveguides as the test structures to determine the GC coupling loss and the propagation loss in the cascades of MZI. The GC pitch was set to 127 μm, determined by the pitch of the polarization maintaining (PM) fiber array utilized for testing. Two different state-of-the-art GCs [30] were used to perform measurements with the TE and TM polarizations since GCs are polarization dependent.

The fabricated devices were measured with an advanced automated optical test setup at the University of British Columbia. Light from a tunable laser was coupled into the test devices via a polished PM fiber array and a grating coupler, and the output was collected in the same way and sent to a photodetector. The transmission spectra of the test structures for the TE and TM polarizations over the wavelength range from 1500 nm to 1583 nm, which was the largest span that could be measured with the tunable laser in the setup, are shown in Fig. 8 and 9. The measurement wavelength range is also limited by the grating couplers used. The reference structures (Ns = 0) loss at a wavelength of 1550 nm is about −15 dB for both polarizations, mainly because of the grating coupler insertion loss and propagation in the bend waveguides, which is identical for all devices.

It is challenging to measure sub 0.5 dB losses from a single device; hence we used cascaded splitters. The peak power at a particular wavelength was extracted from the transmission spectrum as a function of the number of splitters and the excess loss of one device is calculated by determining the slope [9]. Fig. 8(c) shows the loss per splitter as a function of wavelength for both polarizations. The insertion loss varies from 0.17 to 0.37 dB for the TE polarization and from 0.16 to 0.22 dB for the TM polarization. At a wavelength of 1550 nm, the insertion loss of the splitter for the TE polarization is 0.26±0.2 dB and 0.16±0.2 dB for the TM polarization. For the TE polarization, the experimental loss of the device is approximately 0.15 dB more than the simulation results whereas for the TM polarization it is only 0.05 dB more. This difference is most likely because the TE polarization is more sensitive to the sidewall roughness.

The splitter transmission spectra for both arms are shown in Fig. 9(a) and the measured splitting ratio is plotted in Fig. 9(b). A power splitting ratio of 3-dB is achieved for both polarizations over the tested bandwidth. The MZI transmission spectra for both the TE and TM polarizations, excluding the coupling loss is shown in Fig. 9(c). The length difference between the arms of the MZI is 80 μm. From the spectra, an average ER of 25 dB was obtained over a wavelength range of 80 nm for the TE polarization. Also, an average ER of 37 dB over the same wavelength range was measured for the TM polarization. An average ER close to 25 dB indicates that the power splitting ratio is extremely close to 50:50 [6], which matches the simulation results and splitting ratio calculated in Fig. 9(b). The free spectral range is 5 nm for both polarizations.

IV. Conclusion

Many efficient silicon photonic power splitters were reported in the literature and Table 1 below summarize the performance and characteristics for several state-of-the-art devices. They include Y-junction splitters, directional couplers, adiabatic couplers and MMI couplers. This table not only shows the simulated bandwidth and losses, but it also compares the footprint, minimum feature size, polarization behaviour and compatibility with standard commercial silicon photonic fabrication processes. Previously reported designs are limited in at least one of these performance metrics. For instance, splitters with a small footprint are typically not optimized for both polarization and their operating bandwidth can be small. Conversely, broadband and polarization independent power splitters have a large footprint. Other splitters have a very small minimum feature size and a few require a silicon core thickness other than 220 nm. Thus, these

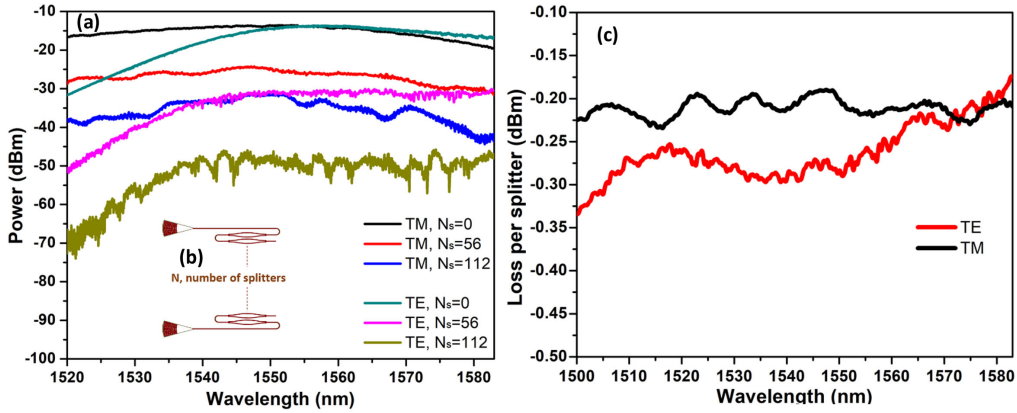

Fig. 8. (a) Measured TE and TM polarization spectra of the cascaded MZIs with a number of splitters Ns = 0, 56, 112. (b) Schematic of the cascaded MZIs used to measure insertion loss. (c). Measure of loss per splitter over the wavelength range 1500nm–1583nm.

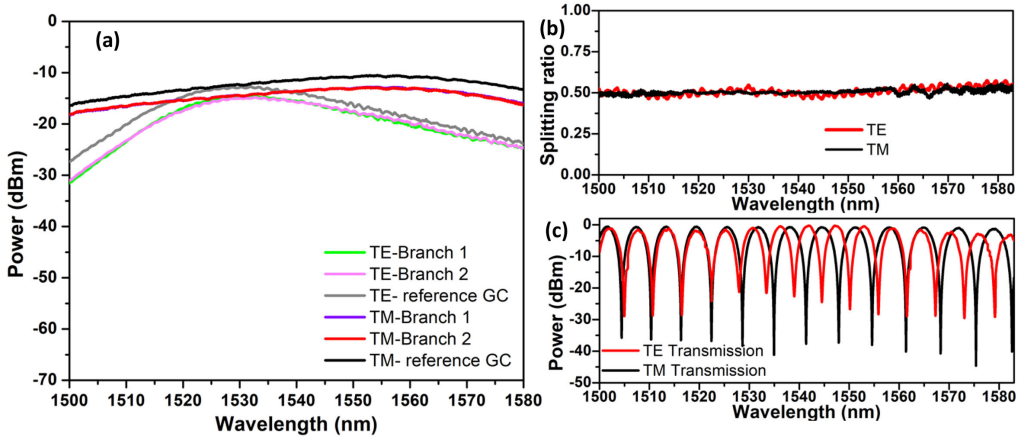

Fig. 9. (a) The transmission spectrum on both arms of splitter for both polarizations. (b) Splitting ratio of splitter for both polarization as a function of wavelength (c)TE and TM transmission curves of the MZI.

TABLE 1
PERFORMANCE COMPARISON OF STATE-OF-THE-ART SPLITTERS WITH PROPOSED DEVICE

Splitter type	Silicon core thickness (nm)	Footprint (μm^2)	Minimum feature size (μm)	Simulated bandwidth (nm)	Polarization and average insertion loss (dB)	Possibility of fabrication through standard CMOS process	Ref.
Y-splitter	220	2x1.4	0.2	1500-1580	TE:0.3	Yes	9
Y-splitter	220	5x2	0.05	1200-1700	TE:0.19 TM:0.14	No	10
Directional coupler	220	15.2x2.3	0.2	1520-1580	TM:0.7	Yes	11
Directional coupler	220	13x6	0.2	1520-1610	TE:0.6 TM:1.1	Yes	12
Directional coupler	220	29.4x0.6	0.4	1500-1600	TE:0.35 TM:0.35	Yes	13
Adiabatic coupler	220	185x30	0.1	1500-1600	NA	No	14
Adiabatic coupler	220	75x2.5	0.1	1500-1600	NA	No	15
Adiabatic coupler	220	25x2	0.1	1500-1600	TE:0.20	No	16
Adiabatic coupler	220	35x7	0.1	1200-1700	TE:0.11	No	17
Adiabatic coupler	220	200x1	0.15	1260-1360	NA	Yes	18
MMI coupler	340	293x6	0.7	NA	TE:0.14	No	20
MMI coupler	320	890x30	NA	NA	NA	No	21
MMI coupler	400	21x8	0.2	NA	TE:0.25	No	23
MMI coupler	220	6.6x2.6	0.3	1500-1600	TE:0.16 TM:0.21	Yes	24
MMI coupler	330	3x1.5	0.2	1520-1600	TE:0.11 TM:0.18	No	25
Proposed design	220	1.8x1.3	0.2	1300-1700	TE:0.26 TM:0.16	Yes	

devices are not compatible with standard commercial fabrication processes.

In comparison with these studies, our device is very compact and can be implemented with commercial fabrication processes.The junction footprint of the proposed splitter is 1.8 × 1.3 μm and the total size of the device including the input waveguides, the multimode region and the output arms is less than 18 μm in length and 4 μm in width. It is broadband (1300–1700 nm) and its performance was measured experimentally over a wavelength range of 80 nm (1500 to 1580 nm). The device exhibits a very low insertion loss of 0.26 dB for the TE polarization and of 0.16 dB for the TM polarization at a wavelength of 1550 nm. Therefore, this splitter is promising for high density photonic applications.

ACKNOWLEDGMENT

The authors thank Silicon Electronic Photonic Integrated Circuit (SiEPIC) for fabricating and testing of the devices and also thank the Centre d'optique, photonique et laser, the Fonds de recherche du Québec–Nature et technologies, and the Natural Science and Engineering Research Council for financial support.

REFERENCES

[1] T. Baehr-Jones, T. Pinguet, P. Lo Guo-Qiang, S. Danziger, D. Prather, and M. Hochberg, "Myths and rumours of silicon photonics," *Nature Photon.,* vol. 6, p. 206, 2012, doi: 10.1038/nphoton.2012.66.

[2] X. Xiao *et al.*, "High-speed, low-loss silicon Mach–Zehnder modulators with doping optimization," *Opt. Exp.,* vol. 21, no. 4, pp. 4116–4125, 2013, doi: 10.1364/OE.21.004116.

[3] Q. Zhao, K. Cui, X. Feng, F. Liu, W. Zhang, and Y. Huang, "Compact and broadband 1 × 4 optical switch based on W2 photonic crystal waveguides," *IEEE Photon. J.,* vol. 8, no. 5, Oct. 2016, Art. no. 7804609, doi: 10.1109/JPHOT.2016.2611699.

[4] H.-C. Chung, K.-S. Lee, and S.-Y. Tseng, "Short and broadband silicon asymmetric Y-junction two-mode (de)multiplexer using fast quasiadiabatic dynamics," *Opt. Exp.,* vol. 25, no. 12, pp. 13626–13634, 2017, doi: 10.1364/OE.25.013626.

[5] D. Kwong *et al.*, "On-chip silicon optical phased array for two-dimensional beam steering," *Opt. Lett.,* vol. 39, no. 4, pp. 941–944, 2014, doi: 10.1364/OL.39.000941.

[6] J. Wang *et al.*, "Novel ultra-broadband polarization splitter-rotator based on mode-evolution tapers and a mode-sorting asymmetric Y-junction," *Opt. Exp.,* vol. 22, no. 11, pp. 13565–13571, 2014, doi: 10.1364/OE.22.013565.

[7] S. Chen, Y. Shi, S. He, and D. Dai, "Compact monolithically-integrated hybrid (de)multiplexer based on silicon-on-insulator nanowires for PDM-WDM systems," *Opt. Exp.,* vol. 23, no. 10, pp. 12840–12849, 2015, doi: 10.1364/OE.23.012840.

[8] T. Li *et al.*, "Low-voltage, high speed, compact silicon modulator for BPSK modulation," *Opt. Exp.,* vol. 21, no. 20, pp. 23410–23415, 2013, doi: 10.1364/OE.21.023410.

[9] Y. Zhang *et al.*, "A compact and low loss Y-junction for submicron silicon waveguide," *Opt. Exp.,* vol. 21, no. 1, pp. 1310–1316, 2013, doi: 10.1364/OE.21.001310.

[10] Y. Wang, S. Gao, K. Wang, and E. Skafidas, "Ultra-broadband and low-loss 3 dB optical power splitter based on adiabatic tapered silicon waveguides," *Opt. Lett.,* vol. 41, no. 9, pp. 2053–2056, 2016, doi: 10.1364/OL.41.002053.

[11] Y. Luo, Y. Yu, M. Ye, C. Sun, and X. Zhang, "Integrated dual-mode 3 dB power coupler based on tapered directional coupler," *Sci. Rep.,* vol. 6, pp. 23516, 2016, doi: 10.1038/srep23516.

[12] J. R. Ong *et al.*, "Broadband silicon polarization beam splitter with a high extinction ratio using a triple-bent-waveguide directional coupler," *Opt. Lett.,* vol. 42, no. 21, pp. 4450–4453, 2017, doi: 10.1364/OL.42.004450.

[13] Y. Kim, M. H. Lee, Y. Kim, and K. H. Kim, "High-extinction-ratio directional-coupler-type polarization beam splitter with a bridged silicon wire waveguide," *Opt. Lett.,* vol. 43, no. 14, pp. 3241–3244, 2018, doi: 10.1364/OL.43.003241.

[14] L. Xu *et al.*, "Polarization independent adiabatic 3-dB coupler for silicon-on-insulator," in *Proc.Conf. Lasers Electro-Opt. (CLEO)*, May 2017, pp. 1–2.

[15] Y. Wang *et al.*, "Polarization-independent mode-evolution-based coupler for the silicon-on-insulator platform," *IEEE Photon. J.,* vol. 10, no. 3, Jun. 2018, Art. no. 4900410, doi: 10.1109/JPHOT.2018.2835767.

[16] L. Xu *et al.*, "Compact high-performance adiabatic 3-dB coupler enabled by subwavelength grating slot in the silicon-on-insulator platform," *Opt. Exp.,* vol. 26, no. 23, pp. 29873–29885, 2018, doi: 10.1364/OE.26.029873.

[17] H. Yun, L. Chrostowski, and N. A. F. Jaeger, "Ultra-broadband 2 × 2 adiabatic 3 dB coupler using subwavelength-grating-assisted silicon-on-insulator strip waveguides," *Opt. Lett.,* vol. 43, no. 8, pp. 1935–1938, 2018, doi: 10.1364/OL.43.001935.

[18] D. Mao *et al.*, "Adiabatic coupler with design-intended splitting ratio," *J. Lightw. Technol.,* vol. 37, no. 24, pp. 6147–6155, Dec. 2019, doi: 10.1109/JLT.2019.2946948.

[19] C. Burtscher, D. Seyringer, and M. Lucki, "Study of the optical properties of 1×16 splitter based on Y-branch and MMI approaches," in *Proc. 18th Int. Conf. Transparent Opt. Netw. (ICTON)*, Jul. 2016, pp. 1–4, doi: 10.1109/ICTON.2016.7550642.

[20] M. S. Rouifed *et al.*, "Ultra-compact MMI-based beam splitter demultiplexer for the NIR-MIR wavelengths of 1.55 μm and 2 μm," *Opt. Exp.,* vol. 25, no. 10, pp. 10893–10900, 2017, doi: 10.1364/OE.25.010893.

[21] N. Najeeb, Y. Zhang, C. J. Mellor, and T. M. Benson, "Design, fabrication and demonstration of a 1x20 multimode interference splitter for parallel biosensing applications," *J. Phys.: Conf. Ser.,* vol. 679, no. 1, 2016, Art. no. 012027.

[22] J. Lee *et al.*, "Compact inp-based 1×2 MMI splitter on si substrate with BCB wafer bonding for membrane photonic circuits," in *Proc. Int. Conf. Indium Phosphide Related Mater.*, Aug. 2012, pp. 8–11, doi: 10.1109/ICIPRM.2012.6403304.

[23] G. Z. Mashanovich *et al.*, "Mid-infrared photonics devices in SOI," in *Proc. SPIE*, 2013, vol. 8629, doi: 10.1117/12.2005341.

[24] S. Hassan and D. Chack, "Design and analysis of polarization independent MMI based power splitter for PICs," *Microelectronics J.,* vol. 104, 2020, Art. no. 104887. [Online]. Available: http://www.sciencedirect.com/science/article/pii/S0026269220304869

[25] Z. Xiao *et al.*, "Ultra-compact low loss polarization insensitive silicon waveguide splitter," *Opt. Exp.,* vol. 21, no. 14, pp. 16331–16336, 2013, doi: 10.1364/OE.21.016331.

[26] G. F. R. Chen, J. R. Ong, T. Y. L. Ang, S. T. Lim, C. E. Png, and D. T. H. Tan, "Broadband silicon-on-insulator directional couplers using a combination of straight and curved waveguide sections," *Sci. Rep.,* vol. 7, no. 1, pp. 7246, 2017, doi: 10.1038/s41598-017-07618-6.

[27] L. B. Soldano and E. C. M. Pennings, "Optical multi-mode interference devices based on self-imaging: Principles and applications," *J. Lightw. Technol.,* vol. 13, no. 4, pp. 615–627, Apr. 1995, doi: 10.1109/50.372474.

[28] A. Cleary, S. Garcia-Blanco, A. Glidle, J. S. Aitchison, P. Laybourn, and J. M. Cooper, "An integrated fluorescence array as a platform for lab-on-a-chip technology using multimode interference splitters," *IEEE Sensors J.,* vol. 5, no. 6, pp. 1315–1320, Dec. 2005, doi: 10.1109/JSEN.2005.857880.

[29] A. W. Snyder and J. D. Love, "Fundamental properties of modes," in *Optical Waveguide Theory*. Boston, MA, USA: Springer, 1983, pp. 208–237.

[30] Y. Wang *et al.*, "Focusing sub-wavelength grating couplers with low back reflections for rapid prototyping of silicon photonic circuits," *Opt. Exp.,* vol. 22, no. 17, pp. 20652–20662, 2014, doi: 10.1364/OE.22.020652.